Journal of Zhejiang University-SCIENCE A (Applied Physics & Engineering)
ISSN 1673-565X (Print); ISSN 1862-1775 (Online)
www.zju.edu.cn/jzus; www.springerlink.com
E-mail: jzus@zju.edu.cn

Computational fluid dynamics simulation of the wind flow over an airport terminal building*

Chun-ho LIU[1], Dennis Y. C. LEUNG[†‡1], Alex C. S. MAN[1], P. W. CHAN[2]

([1]*Department of Mechanical Engineering, The University of Hong Kong, Hong Kong, China*)

([2]*Hong Kong Observatory, Hong Kong, China*)

[†]E-mail: ycleung@hku.hk

Received July 24, 2009; Revision accepted Nov. 24, 2009; Crosschecked Apr. 30, 2010

Abstract: Turbulence in the wake generated by wind flow over buildings or obstacles may produce complex flow patterns in downstream areas. Examples include the recirculating flow and wind deficit areas behind an airport terminal building and their potential impacts on the aircraft landing on nearby runways. A computational fluid dynamics (CFD) simulation of the wind flow over an airport terminal building was performed in this study of the effect of the building wake on landing aircraft. Under normal meteorological conditions, the studied airport terminal building causes limited effects on landing aircraft because most of the aircraft have already landed before entering the turbulent wake region. By simulating the approach of a tropical cyclone, additional CFD sensitivity tests were performed to study the impacts of building wake under extreme meteorological conditions. It was found that, in a narrow range of prevalent wind directions with wind speeds larger than a certain threshold value, a substantial drop in wind speed (>3.6 m/s) along the glide path of aircraft was observed in the building wake. Our CFD results also showed that under the most critical situation, a drop in wind speed as large as 6.4 m/s occurred right at the touchdown point of landing aircraft on the runway, an effect which may have a significant impact on aircraft operations. This study indicated that a comprehensive analysis of the potential impacts of building wake on aircraft operations should be carried out for airport terminals and associated buildings in airfields to ensure safe aviation operation under all meteorological conditions and to facilitate implementation of precautionary measures.

Key words: Aviation safety, Building aerodynamics, Computational fluid dynamics (CFD), *k-ε* turbulence model, Tropical cyclone

doi:10.1631/jzus.A0900449 **Document code:** A **CLC number:** TU3

1 Introduction

Recirculation and wake due to wind flow over buildings may induce a variety of uncertainties in the downstream micro-scale wind environment. Laboratory-scale wind tunnel and water channel experiments have commonly been employed to investigate the aerodynamic effects of the wake behind buildings (Okada and Ha, 1992; Szepesi and Lajos, 1998) and have been used to complement field measurements. However, they are costly and time-consuming to conduct with high accuracy and precision. With the increasing computational power-to-cost ratio of modern computer systems, computational fluid dynamics (CFD) techniques are affordable alternatives for examining the aerodynamic effects of buildings on our living environment.

Owing to the cost-effectiveness of CFD, numerous investigations have been performed to study wind behavior in the wake behind buildings. Senthooran *et al.* (2004) used CFD to elucidate the flow-induced pressure fluctuation around a low-rise building at Texas Tech University. Huang *et al.* (2007), using different CFD turbulence models, compared the mean and dynamic wind load on tall buildings. Apart from

‡ Corresponding author

* Project supported by the Committee for Research and Conference Grants (CRCG) of The University of Hong Kong, China

wind load calculations, Krüs *et al.* (2003) used CFD to determine the effects of isolated roughness elements and an industrial complex on the wind environment of an adjacent airfield. Yoshie *et al.* (2005) employed CFD to investigate the pedestrian-level wind behavior behind a high-rise building. Recently, Neofytou *et al.* (2006) focused on the turbulence generated by an obstacle on a wind field and the in-flight conditions over the nearby runway. The objective of the studies by Krüs *et al.* (2003) and Neofytou *et al.* (2006) was to assess the reliability of CFD for the investigation of wind behavior at airports by comparing modeling results and field measurements. Generally, they arrived at a common conclusion that the wake behind a building posed a significant threat to aircraft over a nearby runway. Thus, certain safety criteria and precautionary measures have been recommended for safe aviation operation. These studies considered only rather limited ranges in the background wind speed and direction.

In this study, a comprehensive CFD simulation of the wind flow around an airport terminal building was performed by considering various background wind speeds and directions with respect to the building, including the windy weather associated with a tropical cyclone. We investigated the effects of building wake and recirculation on the surrounding micro-scale wind environment, together with the potential impacts on the landing aircraft over a nearby runway.

2 Methodology

2.1 Computational domain and boundary conditions

CFD modeling was used to elucidate the wind behavior around a hypothetical Y-shaped airport terminal building. The broad layout and general appearance of the building were entered into a CFD pre-processor for mesh generation. A rectangular computational domain was then developed to accommodate the airport terminal building model to perform the CFD simulation (Fig. 1). The size of the computational domain was 3000 m (length)×4000 m (width)×150 m (height). Because of the finite-sized domain, entrance or boundary effects (i.e., flow disturbances induced by the domain boundaries) may affect the replication of the atmospheric wind conditions in the CFD model. Franke and Hirsch (2004) suggested that to minimize these types of errors affecting the test section located in the central core, the height of the highest building H_{max} (=35 m in this study) should be used as the reference unit for defining the minimum distance between the test section and the domain boundaries. The minimum distance in the downstream extent is $15H_{max}$ and in the upstream and lateral extents is $5H_{max}$. For the vertical extent of the computational domain, Krüs *et al.* (2003) and Neofytou *et al.* (2006) used 350 m and 200 m, respectively, in their airfield CFD studies. However, Huang *et al.* (2007) prescribed the domain height as twice the height of the building in their wind loading study. To compromise the demanding spatial resolution close to the airport terminal building (especially the wake) and the limited computational resource, the vertical extent of the computational domain was set at 150 m ($4.3H_{max}$) in this study. Hence, the size of the computational domain was large enough to eliminate the entrance and boundary effects. In addition to the wind flow around and over the airport terminal building, the areas in the vicinity of the runway and the locations installed with anemometers were the major concerns of this study. A larger computational domain covering all the relevant areas was thus developed.

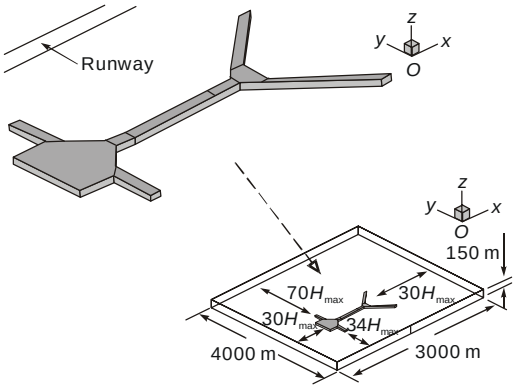

Fig. 1 3D CFD model of the typical airport terminal building and the size of the computational domain

Next, meshes were built for the computational domain. Since rapid changes of wind flow near an airport terminal building are expected, highly refined spatial resolution was applied near the building using unstructured meshes. The total number of elements of the computational domain was about 1.1 million.

2.2 Mathematical model and numerical method

In this CFD model, the fluid is assumed to be incompressible and turbulent, as commonly adopted in environmental fluid mechanics studies under isothermal conditions. Hence, the mathematical model is in the form of Reynolds-averaged Navier-Stokes (RANS) equations that consist of the continuity

$$\frac{\partial \overline{u}_i}{\partial x_i} = 0, \tag{1}$$

and the pseudo steady-state momentum conservation

$$\overline{u}_j \frac{\partial \overline{u}_i}{\partial x_j} = -\frac{1}{\rho}\frac{\partial \overline{p}}{\partial x_i} - \frac{\partial}{\partial x_j}\overline{u_i'' u_j''}. \tag{2}$$

Eqs. (1) and (2) are expressed in the tensor notation and the usual summation convention on repeated indices (i, j=1, 2, 3) applies. The over bars and double prime in the governing equations represent the ensemble averaged and fluctuating components, respectively, that are commonly adopted in RANS turbulence models. The space tensors x_i are the Cartesian coordinates in the streamwise (x), spanwise (y), and vertical (z) directions. The velocity tensors $\overline{u}_i$ are the wind velocity components in the streamwise ($\overline{u}$), spanwise ($\overline{v}$) and vertical ($\overline{w}$) directions, and $\overline{p}$ is the static pressure. Because of the large Reynolds number ($Re=\rho U_{\text{free}} H_{\max}/\mu \approx (1.2\times10\times10)/(1.8\times10^{-5}) \approx 1\times10^6$, where ρ=1.2 kg/m^3 is the air density and μ=1.8×10^{-5} kg/(m·s) is the dynamic viscosity of air at 20 °C and 1 atmospheric pressure), all molecular scale transport processes are neglected. The Reynolds stress

$$-\overline{u_i'' u_j''} = \frac{\mu_t}{\rho}\left(\frac{\partial \overline{u}_i}{\partial x_j} + \frac{\partial \overline{u}_j}{\partial x_i}\right) - \frac{2}{3}k\delta_{ij} \tag{3}$$

is used to handle the unresolved turbulent transport processes by assuming the Boussinesq hypothesis. Here

$$\mu_t = \rho C_\mu \frac{k^2}{\varepsilon} \tag{4}$$

is the turbulent dynamic viscosity (C_μ=0.09 is an empirical modeling constant), k is the turbulent kinetic energy (TKE) ($=\overline{u_i'' u_i''}/2$), ε is the dissipation rate of TKE, and δ_{ij} is the Kronecker symbol. The two-equation k-ε turbulence model (Launder and Spalding, 1972) is employed to close the mathematical model. To close the steady-state RANS equations, the transport equations for the TKE

$$\overline{u}_i \frac{\partial k}{\partial x_i} = \frac{\partial}{\partial x_i}\left(\frac{\mu_t}{\rho\sigma_k}\frac{\partial k}{\partial x_i}\right) + \frac{P_k}{\rho} - \varepsilon, \tag{5}$$

and the TKE dissipation rate

$$\overline{u}_i \frac{\partial \varepsilon}{\partial x_i} = \frac{\partial}{\partial x_i}\left(\frac{\mu_t}{\rho\sigma_\varepsilon}\frac{\partial \varepsilon}{\partial x_i}\right) + \frac{1}{\rho}C_{\varepsilon 1}P_k\frac{\varepsilon}{k} - C_{\varepsilon 2}\frac{\varepsilon^2}{k} \tag{6}$$

in steady-state are solved. Here P_k ($=-\overline{u_i'' u_j''}\partial \overline{u}_i / \partial x_j$) is the TKE production, and σ_k (=1.0) and σ_ε (=1.3) are the effective Prandtl numbers for k and ε, respectively. In this study, the empirical modeling constants in the transport equation for the TKE dissipation rate are $C_{\varepsilon 1}$=1.44 and $C_{\varepsilon 2}$=1.92.

This mathematical modeling procedure was implemented using the commercial CFD code Fluent 6.1 (FLUENT, 2008). The finite volume method with the first-order accurate upwind scheme was used to discretize the transport equations for momentum, TKE, and TKE dissipation rate, while the semi-implicit method for pressure linked equations (SIMPLE) algorithm was used to solve the implicit pressure-velocity coupling in incompressible flow. The resulting systems of algebraic equations are solved by the successive over-relaxation method until the error of the residual is less than 1×10^{-6}.

3 Model validation

A model validation exercise was performed to assess the reliability of the CFD model when used in a study of building aerodynamics before performing the sensitivity tests of the airport terminal building. The wind flow calculated by CFD over and around an isolated high-rise building was compared with a set of wind tunnel results available from the literature as described below.

3.1 Wind tunnel measurements

Yoshie *et al.* (2005) investigated the pedestrian-level wind environment behind an isolated high-rise building. Selected velocity profiles on the horizontal (z=0.125B) and vertical center (y=0) planes in the wake of the building were measured in a wind tunnel (Fig. 2). The width of the square-prism building model B (=0.08 m) also served as the characteristic length scale. The vertical wind profile at the inlet of the wind tunnel is approximated by the power law:

$$\bar{u} = U_{\text{free}} \times \left(\frac{z}{L_z} \right)^{0.27}, \tag{7}$$

where U_{free} is the free-stream wind speed, and L_z is the vertical extent of the wind tunnel. The exponent 0.27 in Eq. (7) represents the wind flow conditions over urban roughness under neutral atmospheric conditions. The free-stream wind speed, which also served as the characteristic velocity scale, was prescribed as U_{free}=6.94 m/s in accordance with the wind tunnel configuration.

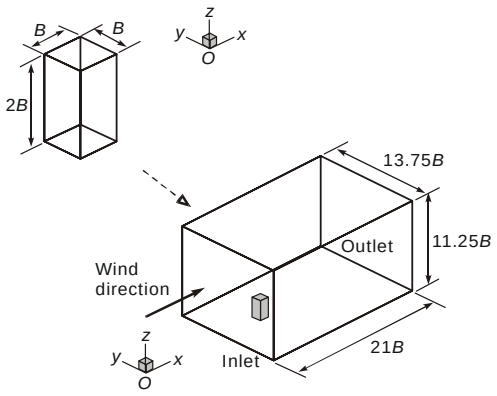

Fig. 2 Dimensions of the high-rise building model used in the wind tunnel experiment and the size of the computational domain

3.2 Computational fluid dynamics model

The sizes of the building model and the computational domain for this model validation exercise were exactly the same as those used in the wind tunnel experiment (Yoshie *et al.*, 2005). Both structured hexahedral and unstructured tetrahedral meshes were used in this model validation exercise for full control of spatial resolution. In the areas of most concern close to the building facades, because of the square-prism geometry, fine hexahedral meshes were applied for more stable and faster convergent results. Unstructured tetrahedral meshes were applied in the areas of less concern (Kim and Boysan, 1999). This configuration of discretization yields almost 660 000 elements.

3.3 Result comparison

Comparison with wind tunnel measurement was made on the vertical (x-z) center plane (y=0) (streamwise $\bar{u}$ (Fig. 3a) and vertical $\bar{w}$ (Fig. 3b) and on the elevated horizontal (x-y) plane at z=0.125B (streamwise $\bar{u}$ (Fig. 4a) and spanwise $\bar{v}$ (Fig. 4b). The CFD results agree reasonably well with the wind tunnel measurements and thus support the reliability of the CFD model being employed in this study.

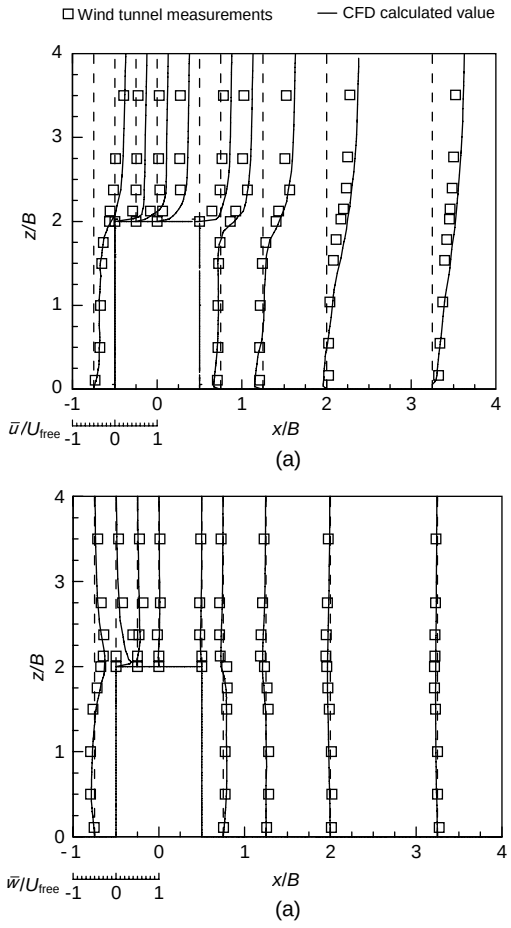

Fig. 3 Comparison of the wind velocity components between the wind tunnel measurements and the CFD calculated values on the vertical (x-z) center plane (y=0). (a) Streamwise $\bar{u}$ and (b) vertical $\bar{w}$ wind velocity components

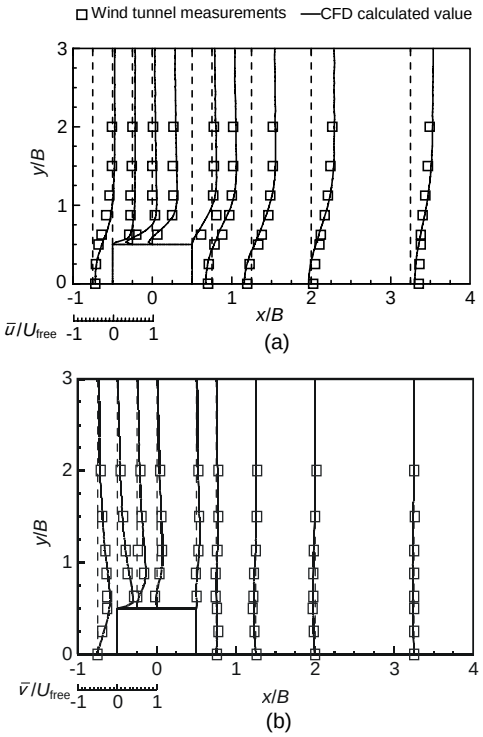

Fig. 4 Comparison of the wind velocity components between the wind tunnel measurements and the CFD calculated values on the elevated horizontal (*x*-*y*) plane at *z*=0.125*B*. (a) Streamwise $\bar{u}$ and (b) horizontal $\bar{v}$ wind velocity components

4 Results and discussion: terminal building simulations

4.1 Preliminary study

In this section, the major concern is the effects of the wake behind the airport terminal building on landing aircraft over the nearby runway. Four prevalent wind directions, namely Θ=0°, 22.5°, 45° and 60° with respect to the airport terminal building, were simulated (Fig. 5). As a preliminary study, a power-law wind profile in the form of $\bar{u} \propto z^{0.27}$ was prescribed at the inlet of the computational domain. Note that the simulated airport is located in a suburban area with rough terrain. Thus, the exponent 0.27 may be overestimated causing a higher wind speed at higher altitude in the simulation. Analogous to Eq. (7), the following wind profile

$$\bar{u} = 22.97 \times z^{0.27} \tag{9}$$

was adopted so that the maximum wind gust at an altitude of 10 m above ground (standard height of wind measurement for meteorological purposes) was 42.8 m/s and at 35 m (the highest point of the airport terminal building) was 60 m/s to simulate an extremely windy condition, e.g., a tropical cyclone with hurricane wind force. The spatial contours of the streamwise velocity components $\bar{u}$ on the horizontal (*x*-*y*) plane at an altitude of *z*=10 m for the four wind directions are shown in Fig. 6. The blue contours represent negative streamwise velocity that outlines the recirculation regions located downstream from the airport terminal building. A number of areas with strong reverse wind flow (up to 15 m/s) can be seen behind the airport terminal building but they do not reach the runway. However, several sharp peaks of velocity contours, induced by the wake behind the airport terminal building, appear over the runway. These findings signify that substantial variations in wind speed in certain areas over the runway could be experienced by aircraft landing under such windy conditions. However, in real life situations, aircraft would not land in these conditions because the operating limits of crosswind/tailwind for a typical aircraft would be exceeded.

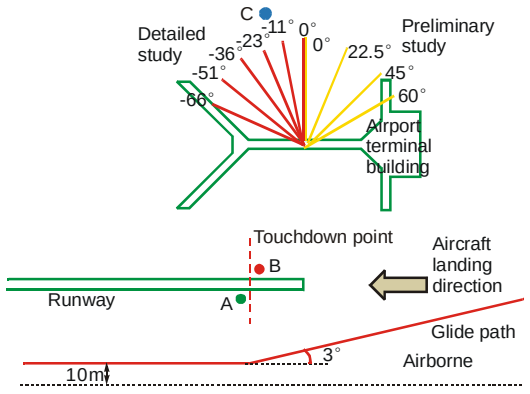

Fig. 5 Four wind directions at Θ=0°, 22.5°, 45°, and 60° in the preliminary study and the six wind directions at Θ=0°, −11°, −23°, −36°, −51°, and −66° in the detailed study. Also shown are the touchdown point on the runway and the glide path of the landing aircraft, and the locations of the anemometers A, B, and C assigned for this study. In this schematic diagram, the airport terminal building and the runway are viewed from the top, and the glide path of the aircraft is viewed from sideway

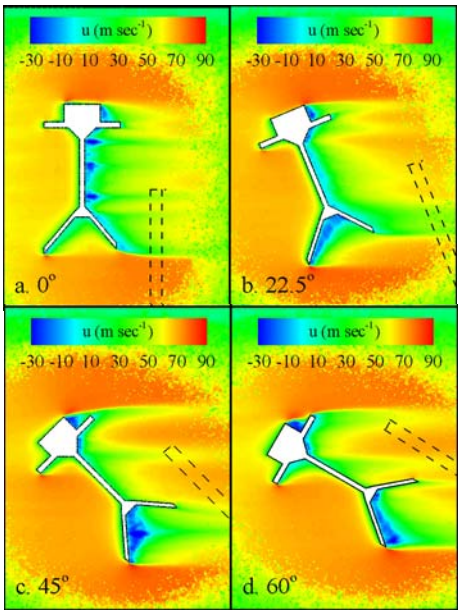

Fig. 6 Spatial contours of the CFD calculated streamwise wind velocity components $\bar{u}$ for different prevailing wind directions (a) Θ=0°; (b) Θ=22.5°; (c) Θ=45° and (d) Θ=60° with respect to the building's orientation. The runway nearby being studied is outlined by the dashed line

4.2 Detailed study

We focused on six scenarios (wind directions) in which the landing aircraft remains airborne close to the runway (Fig. 5). Instead of the idealized power-law used in the last section, the wind profile in a typical tropical cyclone condition was adopted. The wind profile data used, including wind speed and direction, expressed as a function of altitude up to 150 m (Table 1), were based on actual wind measurements in a real tropical cyclone. One of the characteristics of this wind profile is the continuously changing wind direction between the elevations of 14 m and 116 m.

Table 1 Wind profile data in a real tropical cyclone case

Height (m) (AMSL)*	Wind speed (m/s)	Wind direction**
14	19.5	−23°
116	21.4	−57°
150	21.7	−53°

* AMSL: above mean sea level; ** With respect to the orientation of the airport terminal building in Fig. 5

In subsection 4.1, for simplicity, all the ground features surrounding the airport terminal building were ignored. For more realistic simulations in this subsection, different types of ground surfaces, including sea, grassland, asphalt, and concrete, around the airport terminal building were included in the CFD model (Fig. 7). Because of different roughness (Table 2), wind blowing across these surfaces behaves differently. Owing to our limited computational resources, other buildings that may typically be found in close proximity to an airport terminal building were not included.

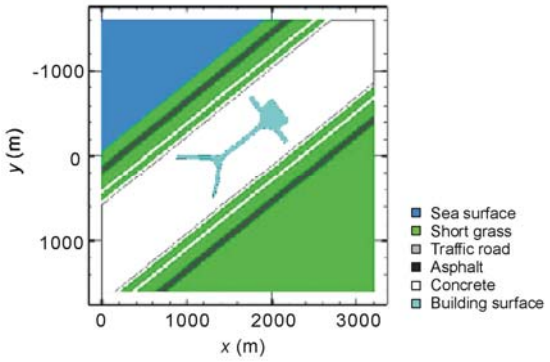

Fig. 7 Modified CFD model of the typical airport terminal building employed in the detailed study in which different types of ground surfaces are included

Table 2 Roughness length for different types of ground surfaces

Surface type	Roughness length (m)
Sea surface	0.0002
Asphalt	0.0024
Traffic road	0.0040
Short grass	0.0100
Building surface	0.0200
Concrete	0.0240

Apart from the wake region behind the airport terminal building, the areas around the runway and the locations of anemometers were the major concern of this study. Higher spatial resolution was thus purposely built over these regions in the modified computational domain. As a result, the number of elements increased to more than 2.1 million. A series of CFD sensitivity tests were performed to examine any differences in the anemometer readings or wind behavior around and over the airport terminal building.

4.2.1 Anemometer readings

A number of anemometers are installed along a runway to monitor the winds for operational purposes. Wind measurements at three anemometers, namely, A, B and C (Fig. 5), were studied to determine the impact of the wake behind the airport terminal building on the wind condition at the airport. From actual wind measurements in tropical cyclone cases, there are several major findings: (1) The three anemometers, though located closely to each other in the airport, recorded significant differences in wind speed; (2) The difference in the wind speed changed significantly with the prevalent wind direction; (3) The maximum difference in wind speed among the 3 anemometers was identified in the wind direction $-36°\leq\Theta\leq-11°$ with respect to the orientation of the airport terminal building.

Since these anemometers are installed along the runways, differences in the wind speed readings could imply potential impacts on the landing aircraft. Therefore, comparison of the CFD calculated wind speed with the anemometer measurements is worthwhile.

1. Comparison of wind speeds between anemometers A and B

A CFD control experiment (free-stream wind speed 21.7 m/s and wind direction $\Theta=-23°$) was conducted in which the airport terminal building was removed from the computational domain. In the absence of the building, the wind speeds at the anemometers A and B were expected to be similar. Interpolating the wind profiles at the height of the anemometers (10 m above ground) revealed that the CFD calculated wind speeds at the anemometers A and B were 18.4 m/s and 18.7 m/s, respectively. This small difference (0.3 m/s, less than 2% of the wind speeds themselves) can be attributed to the drag loss due to surface roughness for wind blowing over a longer distance (about 150 m) from B to A (Fig. 5).

Additional CFD sensitivity tests were carried out in the presence of the airport terminal building under different prevalent wind directions (Fig. 8). The wind speed difference was small when the wind direction was $-66°\leq\Theta\leq-51°$. Shifting the wind direction to $-36°\leq\Theta\leq-11°$ significantly increased the difference in wind speed by from 13% to 25%. Such a magnitude of percentage difference in the wind speeds between A and B has been observed in a real tropical cyclone. Further shifting the wind direction to 0° eventually reduces the difference in wind speed. Therefore, as

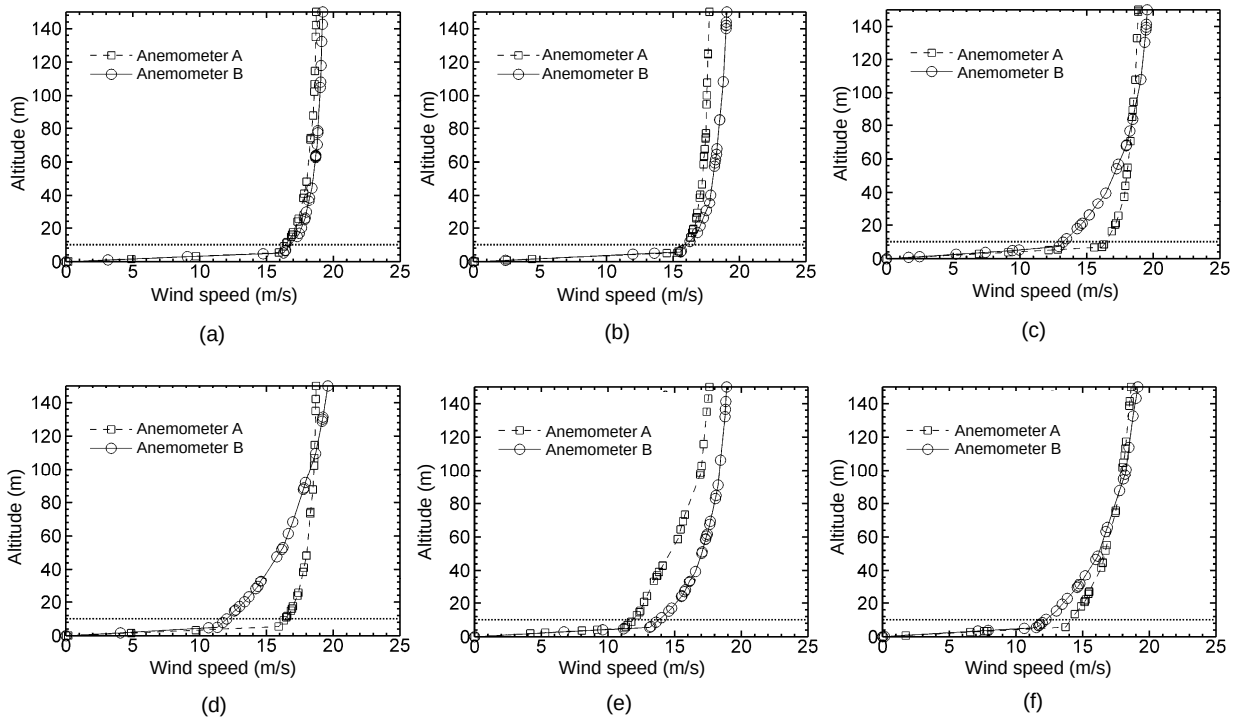

Fig. 8 CFD calculated wind speed profiles at the locations of the anemometers A and B in the presence of the airport terminal building under different prevailing wind directions. (a) −66°; (b) −51°; (c) −36°; (d) −11° and (f) 0°

shown by the CFD results and field measurements, the presence of the airport terminal building apparently affects the readings of the anemometers A and B even though they are only about 150 m apart.

2. Comparison of wind speeds between anemometers A and C

We also compared the readings of the anemometers A and C installed across the airport terminal building (Fig. 5). Similar to the last comparison, a CFD control experiment (free-stream wind speed 21.7 m/s and wind direction Θ=−23°) was conducted in the absence of the airport terminal building and the wind speeds at the two locations were almost the same (16.8 m/s and 17.2 m/s at A and C, respectively). Again, this small wind speed difference is caused mainly by surface roughness. The much larger differences in reality between the readings of the two anemometers are likely caused by the presence of the airport terminal building.

In the case of a real tropical cyclone, the average wind speeds at the anemometers A and C were about 12.86 m/s and 19.24 m/s, respectively, viz. a difference of 6.38 m/s. The CFD simulation for the same wind direction (Θ=−23° with respect to the building) was performed and the wind speeds at 10 m altitude at the anemometers were interpolated (Table 3). The wind speed difference between the anemometers A and C was 7 m/s, which is comparable to the field measurement. The CFD simulation thus shows that the airport terminal building induces a wake with wind speed deficit extending to the runway.

Table 3 Field measured and CFD calculated wind speeds at anemometers A and C

Anemometer	Wind speed at an altitude of 10 m (m/s)	
	Field measurements	CFD calculated results
A	12.86	12.00
C	19.24	19.00
Difference	−6.38	−7.00

4.2.2 Wind flow over the airport terminal building

The sensitivity of the characteristics of the building wake to the prevalent wind direction and the effects on the operation of the landing aircraft are discussed.

1. Glide path

To investigate the effects of the wake of the airport terminal building on the wind conditions encountered by the landing aircraft, the glide path was introduced, viz. the flight path followed by the landing aircraft over the runway being studied. When an aircraft is going to land on the runway, it approaches the touchdown point at an inclination of 3° to the ground surface (Fig. 5). After the aircraft has landed successfully, it decelerates along the runway. A height of 10 m above the runway surface was assumed as the path of the aircraft.

2. 7-knot criterion

As shown above, a wake is developed behind the airport terminal building where the perturbed wind speed could be lower than the unperturbed background speed. While a landing aircraft is traveling into this wake region, it would experience variations in the wind speed. A decrease in headwind resulting from wind variation, if sustained for more than a few seconds, could lead to a drop in the lifting force of the aircraft. In these circumstances, the pilot may need to take corrective action to restore the aircraft back to the intended glide path. However, a change in crosswind may cause a combination of roll and yaw in the aircraft. The roll may result in ground strikes of the aircraft wings especially at low altitudes. This may cause a serious accident. If the wind changes were not persistent, no significant changes to the lift of the aircraft and the intended glide path would occur. A study of the airport structures in the Netherlands (Krüs and Eisenga, 1999) established a 7-knot criterion: a perturbed wind speed deviating from the unperturbed wind speed by 7 knots (or 3.6 m/s) or more could be significant for the normal operation of the aircraft. Moreover, if this wind speed difference of 7 knots is greater than 3 standard deviations of the wind speed, it is considered to arise from some artificial structures, such as a building rather than from the natural variability of the wind.

To investigate the wind situations that would be experienced by the landing aircraft over the runway, the wind speed profile along the glide path was traced from the CFD results. In addition to the perturbed wind profiles, the unperturbed wind profiles (the wind speeds along the glide path in the absence of the airport terminal building) were compared to see whether the 7-knot criterion was exceeded. CFD simulations were performed for six angles of prevalent wind

directions, including −66°, −51°, −36°, −23°, −11°, and 0° with respect to the orientation of the airport terminal building in both the absence and the presence of the building.

3. Wind direction Θ=−66°

The spatial contours of the CFD calculated streamwise wind velocity component at an altitude of 10 m and Θ=−66° are shown in Fig. 9. The prevalent wind blows over the airport terminal building from the domain inflow on the left-hand side. The solid blue lines outline the runway and the dotted blue lines indicate the touchdown point of the landing aircraft on the runway (Fig. 9). Under this wind direction, the wind speed profiles along the glide path for the perturbed and unperturbed situations overlap almost completely in both the airborne and the landed conditions (Fig. 9). Fig. 9 also shows the magnitude of the wind speed difference between the perturbed and the unperturbed winds. The maximum wind speed difference along the glide path is less than 1 m/s (about 3 standard deviations of the wind speed). Hence, the building wake does not have a considerable impact on the landing aircraft over the runway.

4. Wind direction Θ=−51°

The spatial contours of the CFD calculated streamwise wind velocity component at an altitude of 10 m at Θ=−51° are shown in Fig. 10. Under this wind direction, the wake extends to cover part of the runway. This enlarged building wake subsequently leads to a sharp variation in wind speed over the runway. Hence, while descending along the glide path, the landing aircraft could experience a sudden drop in wind speed and a loss of lifting force. Fig. 10 also compares the wind speed of the perturbed and the unperturbed winds along the glide path. For the perturbed wind, owing to the wake effects induced by the airport terminal building, a sharp drop in wind speed occurs along the glide path. The maximum drop in wind speed is 3.1 m/s at an altitude of 41.7 m. This amounts to more than 3 standard deviations of the wind speed and is not caused solely by natural wind fluctuation. However, this level of drop in wind speed does not violate the 7-knot criterion (i.e., it is less than 3.6 m/s). As such, the loss of lifting force for the aircraft is unlikely to be large enough to affect its normal operation.

5. Wind direction Θ=−36°

Under the prevalent wind direction Θ=−36°, the spatial contours of the CFD calculated streamwise wind velocity component at an altitude of 10 m are shown in Fig. 11. Similar to the case of Θ=−51°, an enlarged building wake is developed over the runway that is located quite close to the touchdown point of the aircraft. The drop in wind speed at Θ=−36° (5.8 m/s at a height of 24 m) is much larger than that at Θ=−51°. Another drop in wind speed (2.5 m/s) is found higher up at an altitude of 66 m (Fig. 11). These two drops in wind speed are both larger than 3 standard deviations of the wind speed, i.e., greater than natural wind speed fluctuations. The second drop in wind speed (2.5 m/s), which is less than 7 knots, would not impact significantly on the landing aircraft whereas the first drop in wind speed (up to 5.8 m/s) occurs close to the touchdown point and is greater than 7 knots. Thus, it may affect the normal operation of the aircraft.

6. Wind direction Θ=−23°

Fig. 12 shows the spatial contours of the CFD calculated streamwise wind velocity component at an altitude of 10 m and Θ=−23°. Two sharp peaks in the building wake are found along the glide path. In particular, the largest drop in wind speed (6.4 m/s) occurs right at the touchdown point and is much greater than the 7-knot criterion. Another drop in wind speed (3.8 m/s), which is also greater than 7 knots, takes place when the aircraft is at a height of 40 m. In these circumstances, an aircraft would experience two successive and substantial variations in wind speed as it is descending and preparing to land on the runway, the second occurring near the touchdown point of the runway. Hence, the building wake may affect the normal operation of the landing aircraft.

7. Wind direction Θ=−11°

Under the prevalent wind direction Θ=−11°, the spatial contours of streamwise wind velocity component at an altitude of 10 m are shown in Fig. 13. Two sharp drops in wind speed occur along the glide path. The first drop in wind speed amounts to 4.8 m/s when the aircraft is airborne at an altitude of 43 m. This drop in wind speed is greater than 3 standard deviations of the wind speed and exceeds the 7-knot criterion.

Another drop in wind speed occurs after the

aircraft has landed and beyond the touchdown point on the runway. Though it is up to 5.8 m/s, which is greater than the natural wind speed fluctuation and 7 knots, it would not affect the aircraft as most should have already landed.

8. Wind direction Θ=0°

The last CFD simulated wind direction was Θ=0°. Fig. 14 shows the spatial contours of

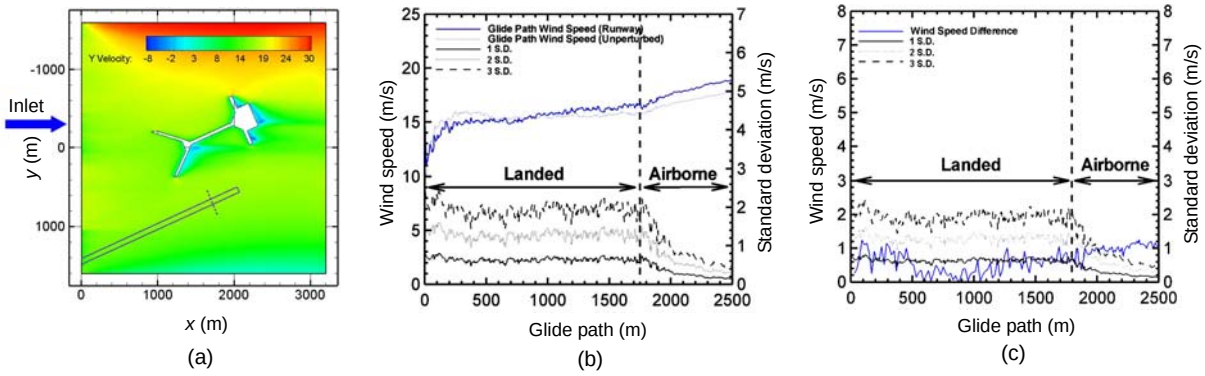

Fig. 9 CFD calculated wind properties in a prevailing wind direction of −66°. (a) Spatial contours of the streamwise wind velocity components at an altitude of 10 m; (b) wind speed and (c) magnitude of wind speed difference along the glide path of a landing aircraft for perturbed and unperturbed wind flow

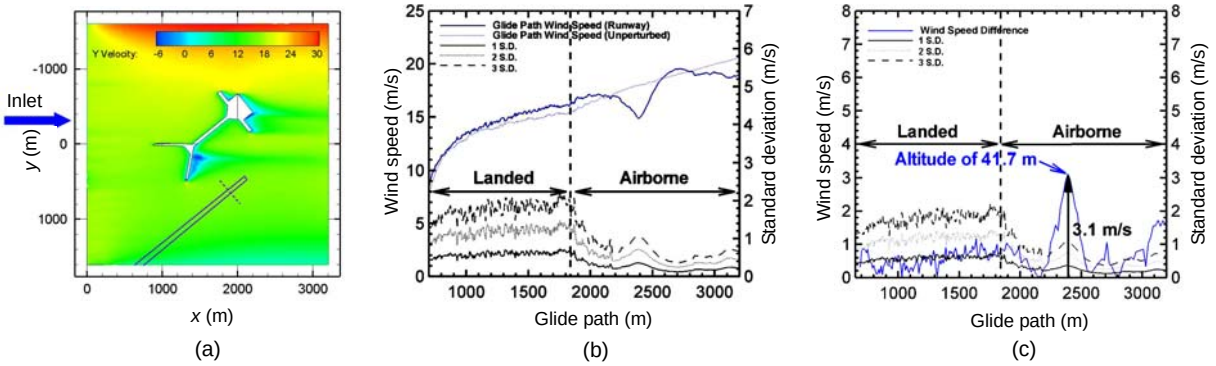

Fig. 10 CFD calculated wind properties in a prevailing wind direction of −51°. (a) Spatial contours of the streamwise wind velocity components at an altitude of 10 m; (b) wind speed and (c) magnitude of wind speed difference along the glide path of a landing aircraft for perturbed and unperturbed wind flow

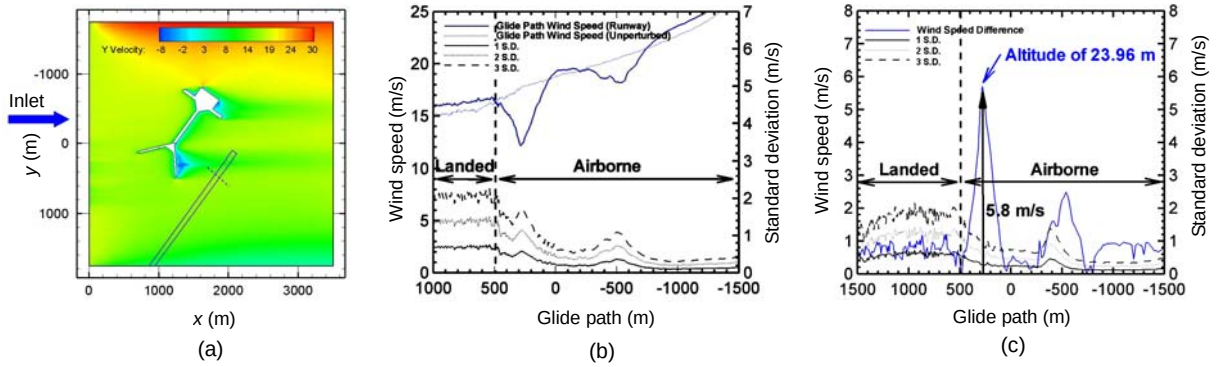

Fig. 11 CFD calculated wind properties in a prevailing wind direction of −36°. (a) Spatial contours of the streamwise wind velocity components at an altitude of 10 m; (b) wind speed and (c) magnitude of wind speed difference along the glide path of a landing aircraft for perturbed and unperturbed wind flow

streamwise wind velocity component at an altitude of 10 m. Three sharp drops in wind speed can be seen along the glide path. Two of them occur when the aircraft is still airborne while the third occurs after landing. The airborne aircraft experiences a drop in wind speed of up to 3.4 m/s (Fig. 14). This drop is greater than 3 standard deviations of the wind speed but does not violate the 7-knot criterion. The last drop

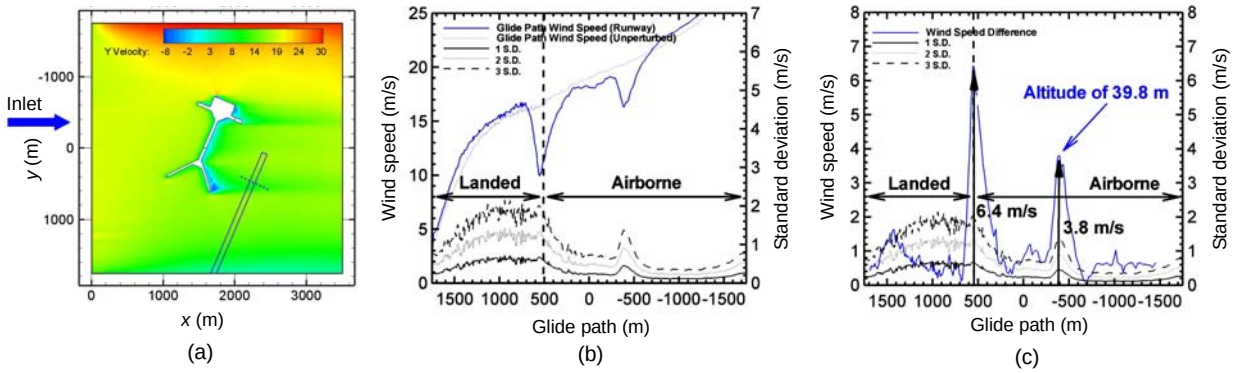

Fig. 12 CFD calculated wind properties in a prevailing wind direction of −23°. (a) Spatial contours of the streamwise wind velocity components at an altitude of 10 m; (b) wind speed and (c) magnitude of wind speed difference along the glide path of a landing aircraft for perturbed and unperturbed wind flow

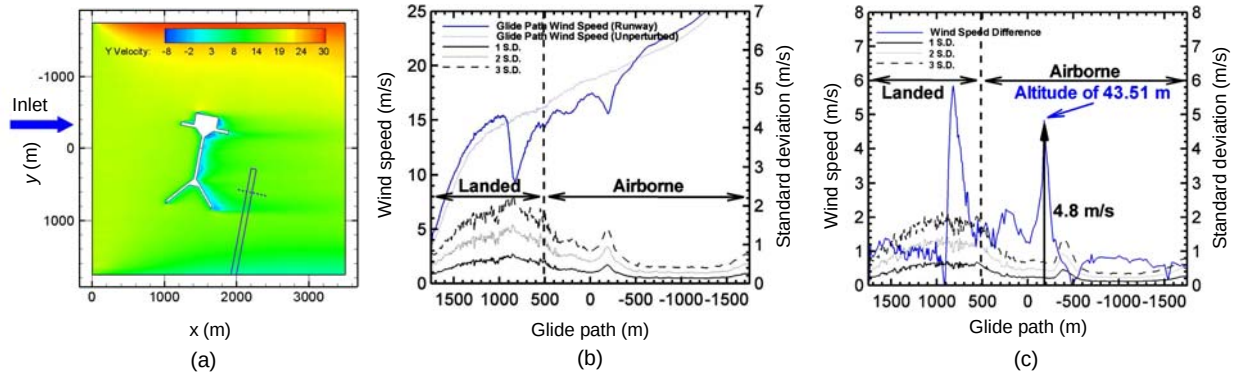

Fig.13 CFD calculated wind properties in a prevailing wind direction of −11°. (a) Spatial contours of the streamwise wind velocity components at an altitude of 10 m; (b) wind speed and (c) magnitude of wind speed difference along the glide path of a landing aircraft for perturbed and unperturbed wind flow

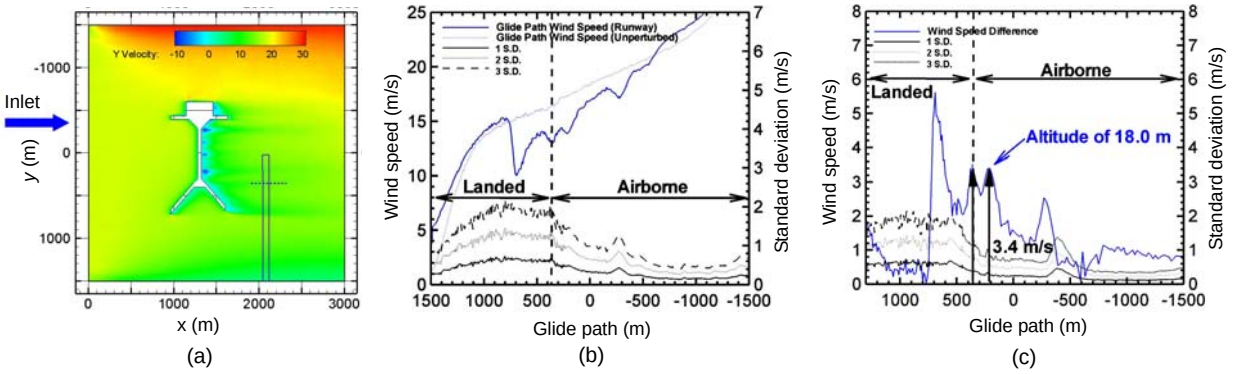

Fig. 14 CFD calculated wind properties in a prevailing wind direction of 0°. (a) Spatial contours of the streamwise wind velocity components at an altitude of 10 m; (b) wind speed and (c) magnitude of wind speed difference in wind speed along the glide path of a landing aircraft for perturbed and unperturbed wind flow

in wind speed amounts to 5.6 m/s and is located beyond the touchdown point on the runway. Hence, it poses virtually no threat to the landing aircraft. As a result, at Θ=0°, these wind speed deficits would not have a significant impact on the landing aircraft.

5 Conclusions

CFD simulations were performed to investigate the aerodynamics and the associated wake effects behind an airport terminal building, together with their potential impacts on aircraft landing on a nearby runway. It was found that, under strong winds (such as those associated with typhoons), a substantial drop in wind speed (more than 3.6 m/s) could be experienced by landing aircraft over the runway for a wind direction in the range of $-36° \leq \Theta \leq -11°$ with respect to the building's orientation. The CFD results showed that the situation is the most significant when the prevalent wind direction is at Θ=−23° with respect to the building's orientation in which the largest drop in wind speed is located very close to the touchdown point of the aircraft on the runway.

There are several limitations of the results reported in this paper. First of all, the building studied in the simulation has a single curving rooftop, instead of a wavy rooftop as may be adopted in a real airport terminal building. Because of limited computing resources, the model domain has a limited size and the model boundary may modify the simulated wind field. Secondly, the CFD tests were carried out assuming steady-state situations, i.e., without natural fluctuations in the background wind direction. In this regard, more sophisticated simulation methods, such as large-eddy simulation, may shed additional light on the building wake effect, especially on rapid wind fluctuations. Thirdly, under tropical cyclone conditions, the strong wind may contain substantial amounts of raindrops, which may induce additional momentum in the wind and affect the aircraft operation. Finally, the simulated results depend on the quality of the numerical model including the accuracy of the numerical methods or mesh quality. For example, in the simulation of the airport terminal building, because of its complicated features, the terminal building was discretized by tetrahedrals. This can ensure that the simulation has reasonable accuracy despite that there are potential drawbacks of the first-order scheme on tetrahedrals. Nonetheless, the results of this paper should provide useful insights for airport authorities around the world for planning new airport buildings. In particular, the potential aerodynamic effects of the airport terminal and other buildings/structures at the airfield on the wind flow along the glide path of the aircraft should be thoroughly studied for the assurance of safe aircraft operations.

References

FLUENT, 2008. FLUENT, ANSYS. Available from http://www.fluent.com [Accessed on May 5, 2009]

Franke, J., Hirsch, C., 2004. Recommendations on the Use of CFD in Wind Engineering. van Beeck, J.P.A.J. (Ed.), Proceedings of the International Conference on Urban Wind Engineering and Building Aerodynamics, COST Action C14, Impact of Wind and Storm on City Life Built Environment. von Karman Institute, Sint-Genesius-Rode, Belgium, p.5-7.

Huang, S., Li, Q.S., Xu, S., 2007. Numerical evaluation of wind effects on a tall steel building by CFD. *Journal of Constructional Steel Research*, **63**(5):612-627. [doi:10.1016/j.jcsr.2006.06.033]

Kim, S.E., Boysan, F., 1999. Application of CFD to environmental flows. *Journal of Wind Engineering and Industrial Aerodynamics*, **81**(1-3):145-158. [doi:10.1016/S0167-6105(99)00013-6]

Krüs, H.W., Eisenga, M., 1999. Numerieke Simulaties van de Omstroming van Gebouwen en de Bijbehorende omgeving. Report, CFD-990801, Cyclone Fluid Dynamics, the Netherlands, p.26 (in Dutch).

Krüs, H.W., Haanstra, J.O., van der Ham, R., Wichers Schreur, B., 2003. Numerical simulations of wind measurements at Amsterdam Airport Schiphol. *Journal of Wind Engineering and Industrial Aerodynamics*, **91**(10):1215-1223. [doi:10.1016/S0167-6105(03)00079-5]

Launder, B.E., Spalding, D.B., 1972. Lectures in Mathematical Models of Turbulence. Academic Press, London, England.

Neofytou, P., Venetsanos, A.G., Vlachogiannis, D., Bartzis, J.G., Scaperdas, A., 2006. CFD simulations of the wind environment around an airport terminal building. *Environmental Modelling & Software*, **21**(4):520-524. [doi:10.1016/j.envsoft.2004.08.011]

Okada, H., Ha, Y.C., 1992. Comparison of wind tunnel and full-scale pressure measurement tests on the Texas Tech Building. *Journal of Wind Engineering and Industrial Aerodynamics*, **43**(1-3):1601-1612. [doi:10.1016/0167-6105(92)90375-K]

Senthooran, S., Lee, D.D., Parameswaran, S., 2004. A computational model to calculate the flow-induced pressure fluctuations on buildings. *Journal of Wind Engineering and Industrial Aerodynamics*, **92**(13):1131-1145. [doi:10.1016/j.jweia.2004.07.002]

Szepesi, Z., Lajos, T., 1998. Wind Tunnel Investigation on Flow and Pollutant Transport past Two Buildings. Proceedings of the 1st Conference on Mechanical Engineering, GEPESZET, Part 2, Budapest, Hungary.

Yoshie, R., Mochida, A., Tominaga, Y., Kataoka, H., Harimoto, K., Nozu, T., Shirasawa, T., 2005. Cooperative Project for CFD Prediction of Pedestrian Wind Environment in the Architectural Institute of Japan. Náprstek, J., Fischer, C. (Ed.), The Fourth European & African Conference on Wind Engineering, ITAM AS CR, Prague.